Table of contents

1. Materials and methods

Reagents and solvents used were commercially available and purchased from Carl ROTH and Aldrich. Preparation and handling of air-sensitive materials were carried out in a N_2 drybox (OMNI-Lab 2 (VAC) or MBraun ULK 1000) with O_2 and H_2O concentrations < 1 ppm.
Mass spectra were performed by electrospray ionization in a high-resolution mass spectrometer Bruker micrOTOF QII (Q-TOF) with a quadrupole analyser with positive and negative ionization modes with a Bruker Cryospray ionization source or by electrospray ionization in an Agilent-1200 mass spectrometer.
UV/Vis absorption spectra were performed by a diode array spectrophotometer Agilent Cary 60 and low temperature control was maintained with a cryostat from Unisoku Scientific Instruments
EPR spectra were recorded with an ESP 300 X-Band EPR spectrometer from Bruker with a TE011 super high Q microwave resonator. Samples were cooled to 77 K with a liquid nitrogen Dewar. Spin quantifications were calculated on the basis of double integrals of the recorded spectra in comparison to a measured Cu^{II}-standard with a given concentration. Sample tubes were filled higher than the cavity dimension to guarantee an equally filled cavity for all measured samples. Spin quantifications were additionally corrected for volume errors resulting in slight differences in tube diameter. EPR simulation was performed with EASYSPIN.[1]
NMR spectra were recorded in a Bruker AV 500 NMR spectrometer or in a Bruker Ultrashield Avance III400 spectrometer.
Methane detection was carried out with an Agilent 7820A GC system equipped with three columns: washed molecular sieves 5Å, 2 m × 1/8 inch outside diameter (OD), Mesh 60/80 SS and Porapak Q, 4 m × 1/8 inch OD, Mesh 80/100 SS, and a thermal conductivity detector.
IR spectra were measured on an ATR unit connected to a Bruker Vector 22 spectrometer under inert atmosphere.
XAS data was collected at the Stanford Synchrotron Radiation Lightsource (SSRL) on beamline 2-2, with the SPEAR3 storage ring operating at 3 GeV and 500mA in top-off mode throughout data collection. Data was collected in unfocused mode using a Si(111) double crystal monochromator for energy selection, which was detuned by 30% to remove contaminating higher harmonics. Samples were maintained at approx. 20K using a He Displex cryostat. XAS spectra were obtained in fluorescence with a 13 element solid-state germanium detector (10 working elements, Ge2, Ge7, and Ge13 nonfunctional). A photodiode placed before I_0 was used to obtain a Cu metal foil reference via scattering, with the first inflection of the Cu metal spectrum set to 8979.0 eV. Data was generally obtained on 1x5 mm (VxH) spots, with individual scans monitored for evidence of photoreduction. No radiation damage was observed, as judged by the lack of any observable changes in the pre-edge and edge features. Data were collected with 10 eV steps before the edge (1 sec integration time), 0.3 eV steps in pre-edge and edge regions (2 sec integration time), and in 0.05k steps over k = 1.62 $Å^{-1}$ to 15 $Å^{-1}$ (integration time increased in k_2-weighted fashion from 2 to 9 sec over range of scan). XAS data was inspected, averaged and normalized using Athena, while EXAFS simulations were conducted using Artemis.[2] EXAFS simulations were performed on k^3-weighted data, with the amplitude reduction factor S_0^2 fixed at 0.9 and ΔE_0 allowed to float at a single common value for all shells. Coordination numbers were varied in integer increments during the simulations, with r and σ^2 allowed to freely float. Cu phase functions were calculated using FEFF6L. Atomic coordinates of the FEFF input files were taken from the DFT model of complex **3**.

Crystal structure determination: Data collection was performed at 100 K on a Stoe IPDS 2Θ diffractometer using Mo-K_α radiation (λ = 0.71073 Å); radiation source was a sealed tube generator with graphite monochromator. Multi-scan (PLATON[3]) absorption correction for **2**. The structure was solved by direct methods (SHELXS-97[4]) and refined by full matrix least-squares procedures based on F^2 with all measured reflections (SHELXL-97[4]). All non-hydrogen atoms were refined anisotropically. H atoms were introduced in their idealized positions and refined as riding except for the N bonded ones which were located in the Fourier electron density map.

2. Computational details

Density functional theory (DFT) calculations were performed with the Gaussian09 program package.[5] The geometry of **3** $[Cu(^{Me}L\text{-}N)]^+$ was optimized with the B3LYP exchange-correlation functional[6, 7] and the TZVP basis set.[8] Copper species were considered in all possible spin states without symmetry constraints. The acetonitrile solvation effects were included in geometry optimizations through the SMD polarizable continuum model.[9]
IR spectra intensities of **3** were simulated at 298 K. The IR spectrum was also modelled with the ^{15}N isotope $[Cu(^{Me}L\text{-}^{15}N)]^+$ compound, to determine the shift in the Cu-N bond stretching frequency due to the isotopic labelling. Mulliken spin densities were computed to rationalize the electronic structure of the copper-nitrene intermediate. The atomic orbital contribution to the SNOs was evaluated with the Multiwfn 3.3.6 software.

3. Synthesis and characterization of ^{H}L-N$_3$ and ^{Me}L-N$_3$

L-Br and ^{Me}L-Br were prepared as previously reported.[10, 11]

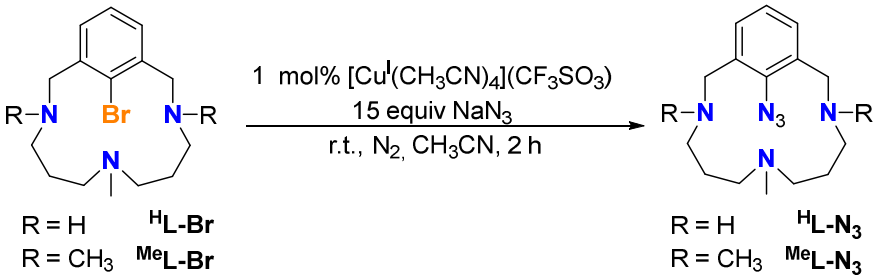

Scheme S1. Synthesis of ^{H}L-N$_3$ and ^{Me}L-N$_3$ by reaction of ^{H}L-Br and ^{Me}L-Br with an excess NaN$_3$ and 1 mol% [Cu^{I}(CH$_3$CN)$_4$](CF$_3$SO$_3$) as catalyst.

Synthesis of ^{H}L-N$_3$. Into the glovebox, ligand ^{H}L-Br (0.0068g, 21 µmol) was dissolved in acetonitrile (1 mL) and this solution was transferred to a vial containing 15 equiv NaN$_3$ (0.020 g, 0.31 mmol). Then, 1 mol% [Cu^{I}(CH$_3$CN)$_4$](CF$_3$SO$_3$) was added (addition of 0.1 mL of a 2.7 mM stock solution in acetonitrile). The colourless solution became slightly red indicating that oxidative addition occurred to afford the red-colored aryl-Cu^{III}-Br complex. The resulting mixture was stirred at room temperature for 2 hours and afterwards the solvent was removed. H$_2$O with NH$_3$ drops (~ 2 mL) were added to the resulting residue and this aqueous mixture was extracted with dichloromethane (3 x 2 mL). The combined organic extracts were dried over MgSO$_4$, filtered and the solvent was removed under vacuum. Ligand ^{H}L-N$_3$ was obtained as a yellow oil (95 %). ^{1}H-NMR (CDCl$_3$, 400 MHz, 298K) δ, ppm: 7.10 (d, J = 7.6 Hz, 2H, Ar**H**), 7.01 (dt, J = 7.6 Hz, 1H, Ar**H**), 4.42 (d, J = 14 Hz, 2H, Ar-C**H**$_2$), 3.52 (d, J = 14 Hz, 2H, Ar-C**H**$_2$), 2.63-2.51 (m, 2H, N-C**H**$_2$), 2.39-2.28 (m, 2H, N-C**H**$_2$), 2.05-1.96 (m, 2H, N-C**H**$_2$), 1.86 (s, 3H, C**H**$_3$), 1.53-1.37 (m, 4H, NCH$_2$-C**H**$_2$-CH$_2$N). ESI-MS (m/z): 289.21 (100) [^{H}L-N$_3$ + H]$^{+}$. FT-IR (ν, cm^{-1}): 2262 (N$_3$).

Synthesis of ^{Me}L-N$_3$. Into the glovebox, ligand ^{Me}L-Br (0.0074 g, 21 µmol) was dissolved in acetonitrile (1 mL) and this solution was transfered to a vial containing 15 equiv NaN$_3$ (0.022 g, 0.34 mmol). Then, 1 mol% [Cu^{I}(CH$_3$CN)$_4$](CF$_3$SO$_3$) was added (addition of 0.1 mL of a 2.7 mM stock solution in acetonitrile). The colourless solution became dark green indicating that oxidative addition occurred to afford the aryl-Cu^{III}-Br complex. The resulting mixture was stirred at room temperature for 1 hour and afterwards the solvent was removed. H$_2$O with NH$_3$ drops (~ 2 mL) were added to the resulting residue and this aqueous mixture was extracted with dichloromethane (3 x 2 mL). The combined organic extracts were dried over MgSO$_4$, filtered and the solvent was removed under vacuum. Ligand ^{Me}L-N$_3$ was obtained as a yellow oil (91 %). ^{1}H-NMR (CDCl$_3$, 400 MHz, 298K) δ, ppm: 7.11 (d, J = 7.2 Hz, 2H, Ar**H**), 6.98 (dt, J = 7.2 Hz, 1H, Ar**H**), 4.07 (d, J = 12 Hz, 2H, Ar-C**H**$_2$), 3.01 (d, J = 12 Hz, 2H, Ar-C**H**$_2$), 2.55-2.50 (m, 2H, NH-C**H**$_2$), 2.36 (s, 6H, C**H**$_3$), 2.35-2.28 (m, 2H, N$_{CH3}$-C**H**$_2$), 1.80 (s, 3H, C**H**$_3$), 1.78-1.65 (m, 4H, NCH$_2$-C**H**$_2$-CH$_2$N), 1.55-1.35 (m, 2H), 1.35-1.15 (m, 2H). ESI-MS (m/z): 317.26 (100) [^{Me}L-N$_3$ + H]$^{+}$. IR: 2261 cm^{-1}.

By analogy to previously reported C_{aryl}-heteroatom bond formation reactions using ^{H}L-Br,[10, 11] formation of ^{H}L-N_3 and ^{Me}L-N_3 presumably occurs through a 2e$^-$ Cu^{I}/Cu^{III} catalytic cycle involving oxidative addition, ligand-exchange and reductive elimination steps (Scheme S2).

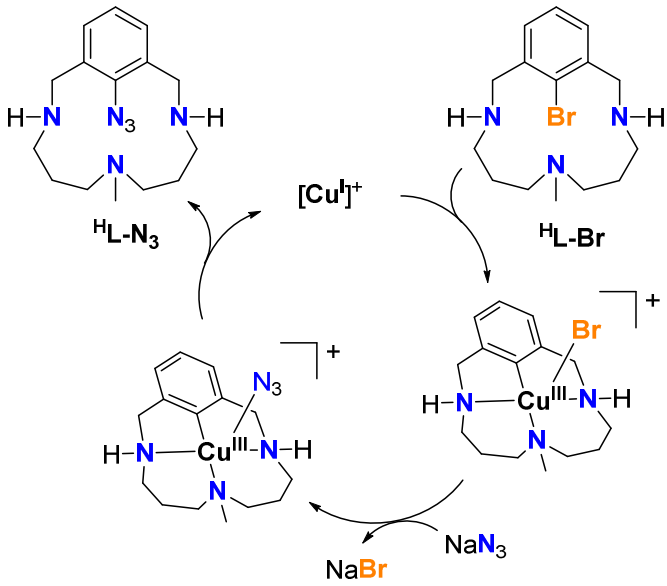

Scheme S2. Cu^{I}/Cu^{III} catalytic cycle for the synthesis of ^{H}L-N_3 from ^{H}L-Br.

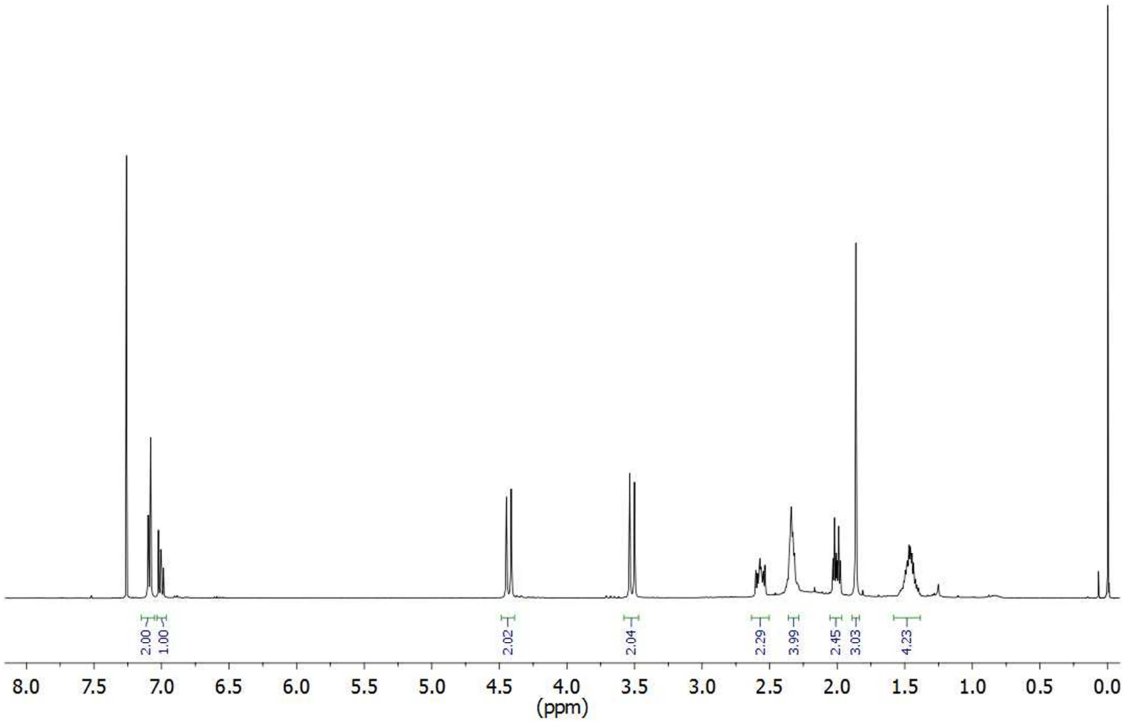

Figure S1. ^{1}H-NMR spectrum of ^{H}L-N_3 in $CDCl_3$ at 298K (400 MHz).

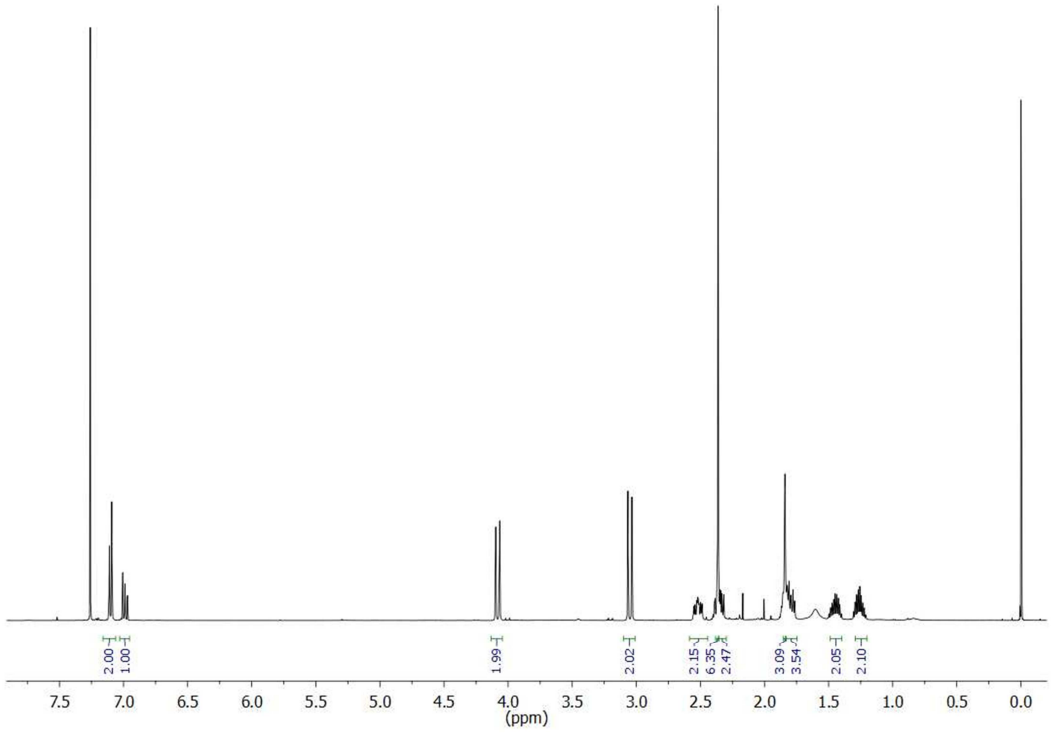

Figure S2. ^{1}H-NMR spectrum of ^{Me}L-N_3 in $CDCl_3$ at 298K (400 MHz).

4. Synthesis and characterization of compound 2

UV/vis monitoring of the reaction of ^{H}L-N$_3$ with Cu^{I} to form compounds 1 and 2. In a typical experiment, 2.5 mL of a 1.4 mM solution of ^{H}L-N$_3$ (3.5 μmols) in acetonitrile were placed in a 1 cm path-length cuvette. The quartz cell was placed in the Unisoku cryostat of the UV/vis spectrophotometer set at 298K. After reaching thermal equilibrium an UV/Vis absorption spectrum of the starting ^{H}L-N$_3$ was recorded. Then, 150 μL of a 31 mM solution of [Cu^{I}(CH$_3$CN)$_4$](CF$_3$SO$_3$) (4.6 μmols, 1.5 equiv) in acetonitrile were added. Initially, a transient species with a band at ~380 nm was formed but it quickly evolved to form compound **2** with a characteristic absorption band at λ_{max} [ε, M^{-1}cm^{-1}] = 550 nm [1000]. Compound **2** was fully formed within 500 s (Figure S3).

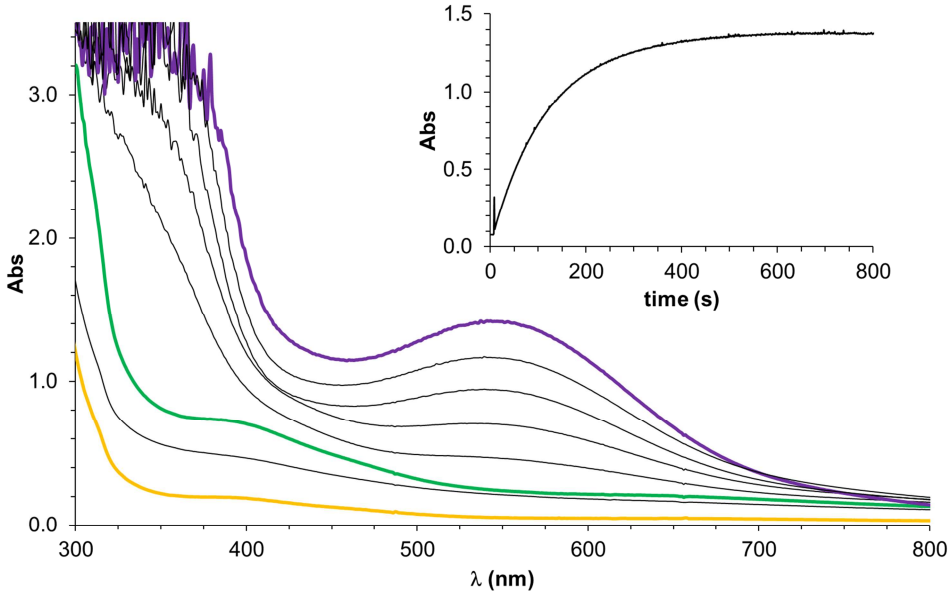

Figure S3. UV/vis absorption spectroscopic changes observed upon reaction of ^{H}L-N$_3$ (yellow line) with 1.5 equiv. of [Cu^{I}(CH$_3$CN)$_4$](CF$_3$SO$_3$) in acetonitrile at 25ºC under Ar to form **1** (green line), which evolves to compound **2** (purple line). Inset: kinetic trace at λ = 550 nm.

Synthesis and isolation of compound 2. Into the glovebox, ligand ^{H}L-N$_3$ (35 μmol) was dissolved in acetonitrile (3 mL) and then [Cu^{I}(CH$_3$CN)$_4$](CF$_3$SO$_3$) (13 mg, 35 μmol) dissolved in the minimum amount of acetonitrile was added. The resulting mixture was stirred at room temperature for 15 min to afford a purple solution. Slow diethyl ether diffusion over the resulting solution at room temperature afforded 9.5 mg of compound **2** as purple crystals suitable for X-ray diffraction (yield 56%). ^{1}H-NMR and ESI-MS of compound **2** are depicted in Figures S4 and S5, respectively.

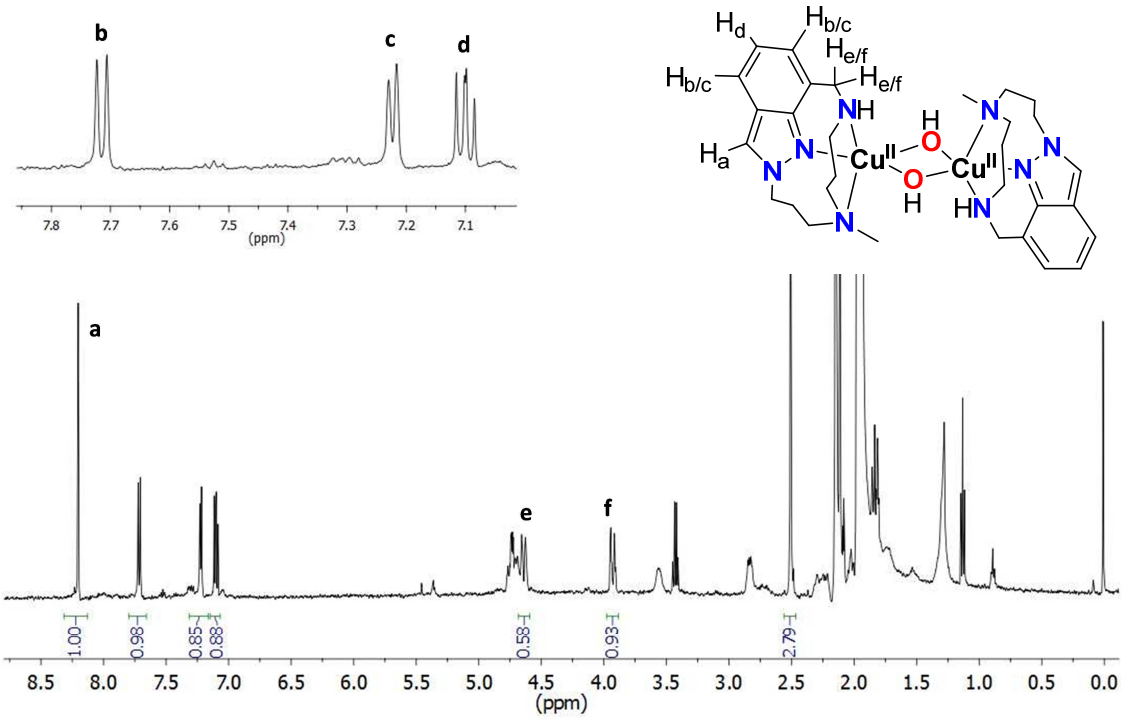

Figure S4. ^{1}H-NMR spectrum of **2** in CD_3CN at 298K (500 MHz).

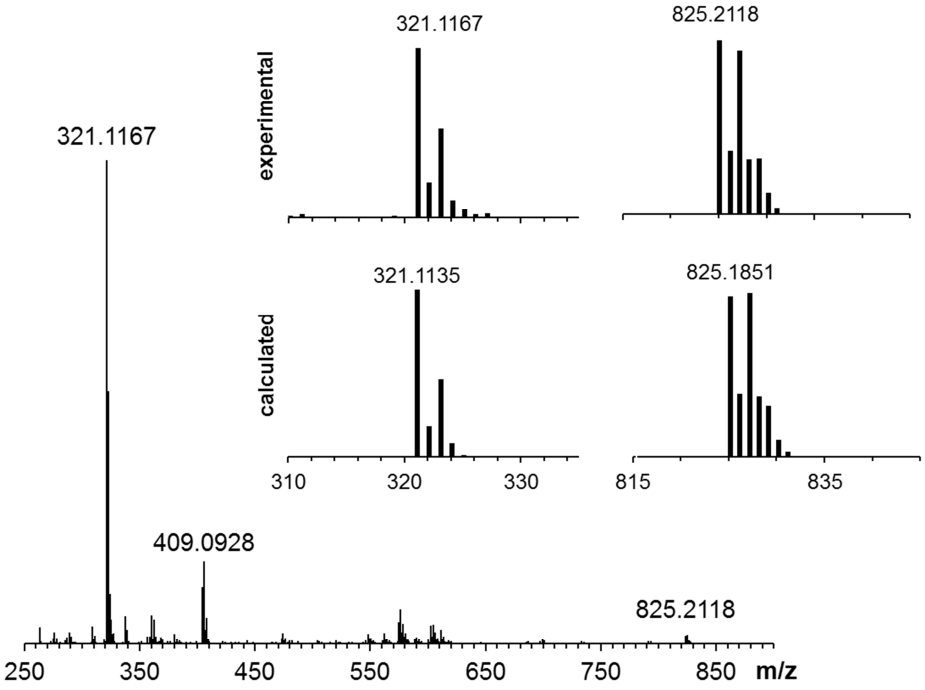

Figure S5. ESI-MS spectrum (3 eV) of isolated compound **2** in acetonitrile at 25ºC under N_2. Inset: experimental pattern and simulation of the most relevant peaks in the MS spectrum of **2**. The peak at m/z 321.1167 corresponds to $[Cu^{I}(L^{in})]^{+}$ while the peak at m/z 825.2118 corresponds to the molecular peak $[Cu^{II}_2(OH)_2(L^{in})_2(CF_3SO_3)]^{+}$.

Table S1. Crystal data for **2**.

Formula weight	975.97
Temperature	100(2) K
Wavelength	0.71073 Å
Crystal system, space group	orthorombic, $P2_1\ 2_1\ 2_1$
Unit cell dimensions	a = 10.9034(3) Å α = 90º
	b = 18.9785(6) Å β = 90º
	c = 19.5583(7) Å γ = 90º
Volume	4047.2 A^3
Density (calculated)	1.602 g/cm^3
Z, Calculated density	4
Absorption coefficient	1.240 mm^{-1}
F(000)	2008
Crystal size	0.24 x 0.12 x 0.05 mm
Theta range for data collection	2.343 to 25.066º
Limiting indices	$-12 \leq h \leq 12$, $-20 \leq k \leq 22$, $-22 \leq l \leq 23$
Reflections collected / unique	16697 / 7126 [R(int) = 0.0723]
Completeness to Θ	99.8% (Θ = 25.00º)
Refinement method	Full-matrix least-squares on F^2
Data / restraints / parameters	7126 / 0 / 532
Goodness-of-fit on F^2	1.031
Final R indices [I>2σ(I)]	R1 = 0.0484 wR2 = 0.1343
R indices (all data)	R1 = 0.0577 wR2 = 0.1424
Largest diff. peak and hole	0.757 and -0.372 $e.A^{-3}$

Table S2. Selected bond lengths (Å) and angles (º) for **2**.

Cu1 O1	1.925(5)	O1 Cu1 O2	76.94(19)
Cu1 O2	1.942(5)	O1 Cu1 N5	100.9(2)
Cu1 N5	1.988(5)	O2 Cu1 N7	90.5(2)
Cu1 N7	2.025(5)	N5 Cu1 N7	87.4(2)
Cu1 N8	2.298(6)	O1 Cu1 N8	96.1(2)
Cu1 Cu2	3.0353(10)	O2 Cu1 N8	107.0(2)
Cu2 O2	1.934(5)	N5 Cu1 N8	94.4(2)
Cu2 O1	1.945(5)	N7 Cu1 N8	96.2(2)
Cu2 N1	1.991(5)	O2 Cu2 O1	76.66(19)
Cu2 N3	2.019(5)	O2 Cu2 N1	101.2(2)
Cu2 N4	2.298(6)	O1 Cu2 N3	90.5(2)
		N1 Cu2 N3	87.4(2)
		O2 Cu2 N4	95.6(2)
		O1 Cu2 N4	106.8(2)
		N1 Cu2 N4	94.8(2)
		N3 Cu2 N4	96.6(2)
		Cu1 O1 Cu2	103.3(2)
		Cu2 O2 Cu1	103.1(2)

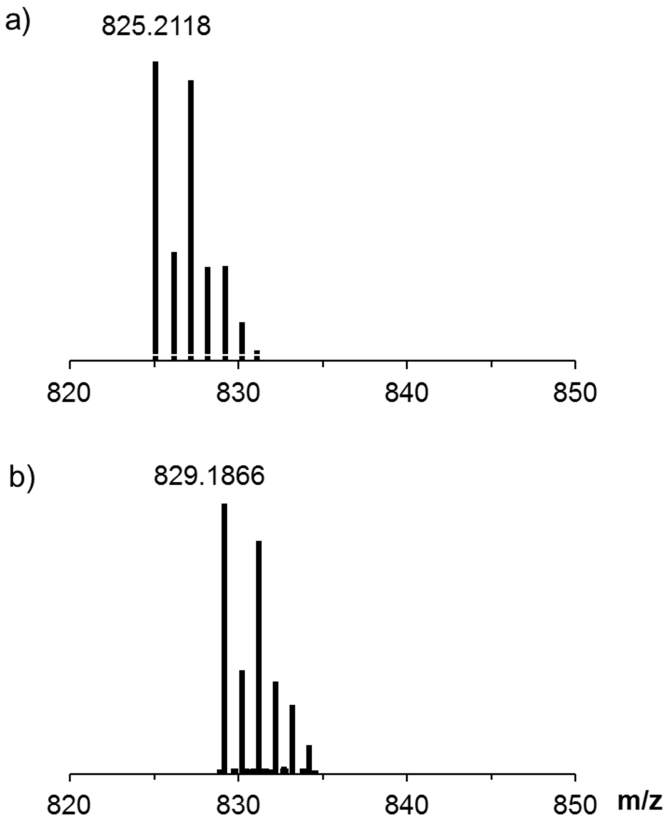

Figure S6. ESI-MS of compound **2** before (a) and after (b) addition of 10 equiv $H_2{}^{18}O$ in acetonitrile at 25ºC under N_2. The molecular peak at m/z 825.21 shifts 4 units (m/z 829.20) due to exchange of the hydroxo ligands with $H_2{}^{18}O$.

5. Synthesis and characterization of compound 1

UV/vis monitoring of the reaction of ^{H}L-N$_3$ with Cu^{I} to form compound 1. In a typical experiment, 2.5 mL of a 1.4 mM solution of ^{H}L-N$_3$ (3.5 µmols) in acetone were placed in a 1 cm path-length cuvette. The quartz cell was placed in the Unisoku cryostat of the UV/vis spectrophotometer and cooled down to 223K. After reaching thermal equilibrium an UV/Vis absorption spectrum of the starting ^{H}L-N$_3$ was recorded. Then, 150 µL of a 31 mM solution of [Cu^{I}(CH$_3$CN)$_4$](CF$_3$SO$_3$) (4.6 µmols, 1.5equiv) in acetonitrile were added. The formation of a band at λ_{max} [ε, M^{-1}cm^{-1}] = 380 nm [615], 790 nm [65] was observed. **1** was fully formed within 1000 s.

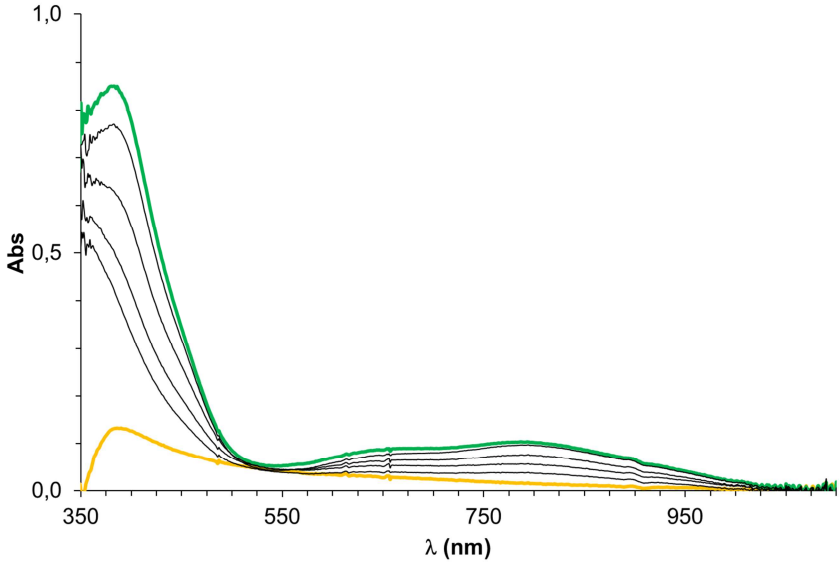

Figure S7. UV/Vis absorption spectroscopic changes observed upon the reaction of ^{H}L-N$_3$ (yellow line) with 1.5 equivalent of [Cu^{I}(CH$_3$CN)$_4$](CF$_3$SO$_3$) in acetone at -50ºC under Ar to form **1** (green line) in 15 min.

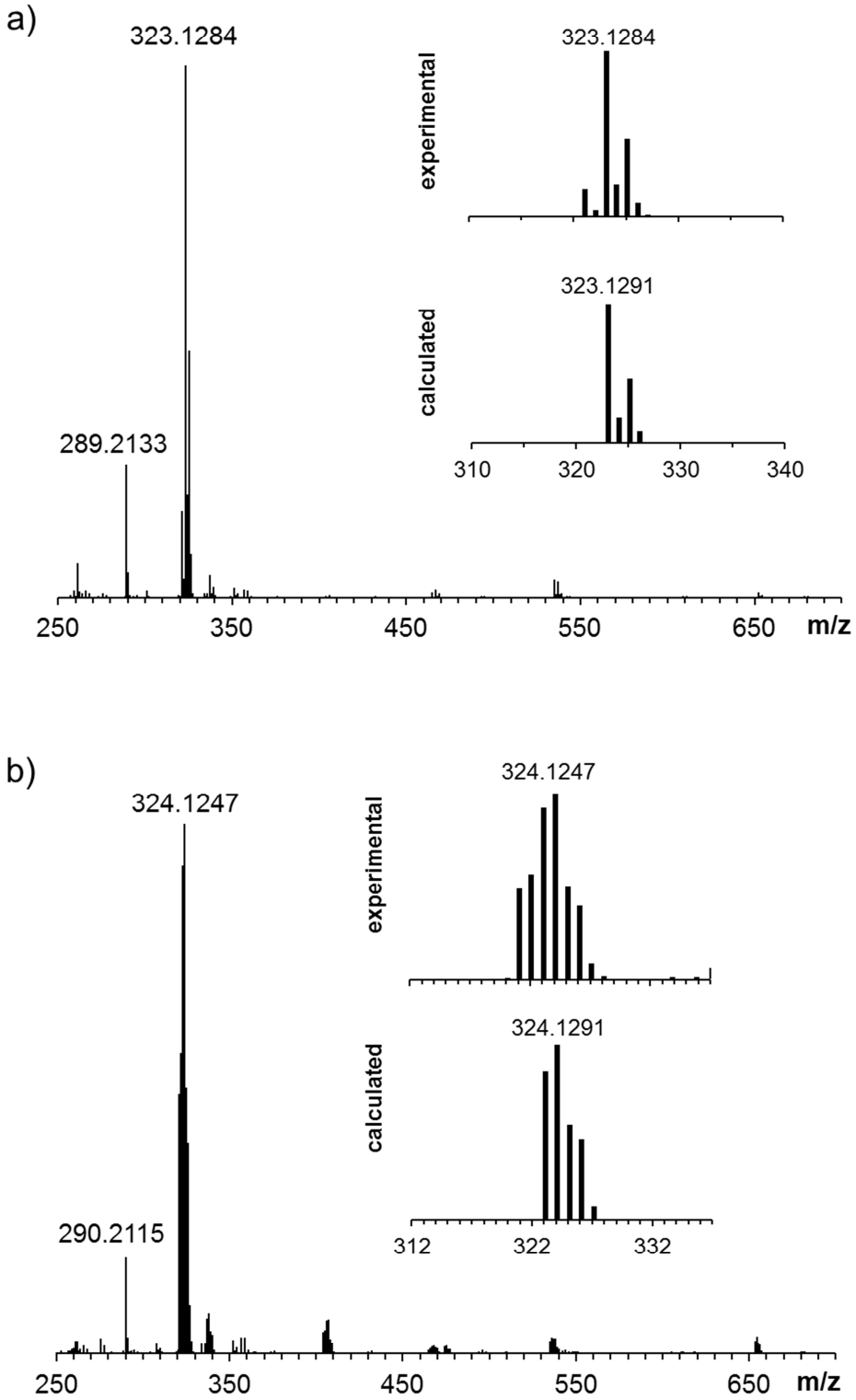

Figure S8. CSI-MS spectra of compound **1** (a) and its 50% ^{15}N-labeled analogue (b) in acetone at -50ºC under N_2. Insets: simulated and experimental molecular peaks of **1** (inset a) and its 50% ^{15}N-labeled analogue (inset b). The discrepancy between experimental and calculated patterns is due to the presence of the decomposition product of **1**. Thus, the ion peak at m/z 321.13 (^{14}N) or 322.13 (^{15}N) corresponds to $[Cu(L^{in})]^+$, which derives from the decomposed species **2**.

6. Generation of compound 3 and XAS analysis

UV/vis monitoring of the reaction of ^{Me}L-N$_3$ with Cu^{I} to form compound 3. In a typical experiment, 2.5 mL of a 1.26 mM solution of ^{Me}L-N$_3$ (3.1 µmols) in acetonitrile were placed in a 1 cm path-length cuvette. The quartz cell was placed in the Unisoku cryostat of the UV/vis spectrophotometer set at 298 K. After reaching thermal equilibrium an UV/Vis absorption spectrum of the starting ^{Me}L-N$_3$ was recorded. Then, 100 µL of a 31 mM solution of [Cu^{I}(CH$_3$CN)$_4$](CF$_3$SO$_3$) in acetonitrile were added (3.1 µmols, 1 equiv). The formation of a band at λ_{max} [ε, M^{-1}cm^{-1}] = 360 nm [1200], 710 nm [200] and 980 nm [150] was observed. **3** was fully formed immediately by irradiation every second.

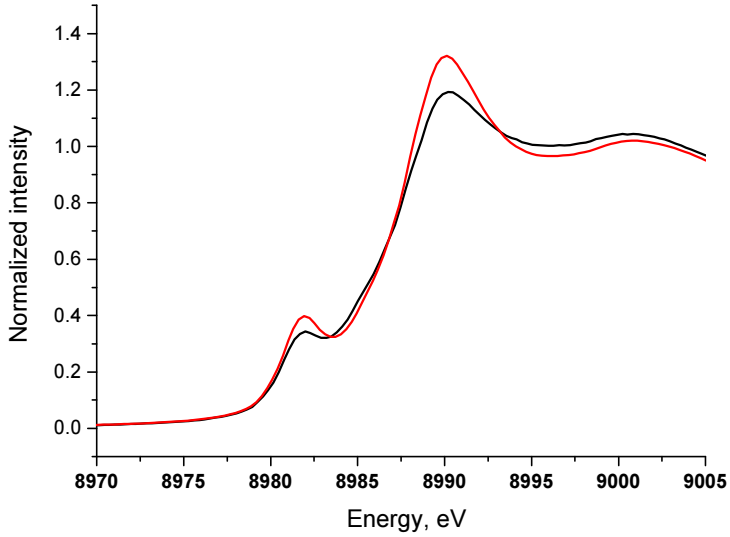

Figure S9. XANES of compounds **2** (red trace) and **3** (black trace) at 20K.

Table S3. Summary of EXAFS fitting for **3**. Bold line represents the best fit for the system (fit 6). Fourier transform range: 2 - 12 Å^{-1}. The fit was optimized in R space with a k-weight of 3. The fitting range is 1.0-2.0 and 1.0-3.0 for fits 1-3 and 4-6, respectively.

	Cu–O/N			Cu–C			Cu–C			
Fit	**N**	**R [Å]**	**σ [Å]**	**N**	**R [Å]**	**σ [Å]**	**N**	**R [Å]**	**σ [Å]**	**R_F**
1	3	2.01	0.002							.026
2	4	2.01	0.005							.009
3	5	2.00	0,007							.035
4	4	2.01	0.006							**.181**
5	4	2.04	0.005	2	2.43	0.006				.162
6	**4**	**2.04**	**0.007**	**2**	**2.44**	**0.006**	**12**	**3.23**	**0.009**	**.007**
DFT	**4**	**2.08**		**2**	**2.53**		**12**	**3.45**		

Table S4. Summary of EXAFS fitting for **2**. Bold line represents the best fit for the system (fit 7). Fourier transform range: 2 - 12 $Å^{-1}$. The fit was optimized in R space with a k-weight of 3. The fitting range is 1.0-2.0 and 1.0-3.15 for fits 1-4 and 5-7, respectively.

	Cu–O/N			Cu–O/N			Cu–Cu			Cu–C				
Fit	**N**	**R [Å]**	**σ [Å]**	**N**	**R [Å]**	**σ [Å]**	**N**	**R [Å]**	**σ [Å]**	**N**	**R [Å]**	**σ [Å]**	**R_F**	**reduced chi-square**
1	2	1.97	0.003										.051	87
2	4	1.97	0.008										.020	34
3	4	1.99	0.007	1	2.10	0.001							.019	29
4	5	2.18	0.004										.267	38
5	4	1.99	0.008	1	2.13	0.008							.120	52
6	4	1.99	0.008	1	2.13	0.008	1	2.91	0.007				.040	25
7	**4**	**1.99**	**0.008**	**1**	**2.13**	**0.008**	**1**	**2.93**	**0.007**	**6**	**3.30**	**0.007**	**.014**	**20**
DFT	**4**	**1.97**		**1**	**2.29**		**1**	**3.03**						

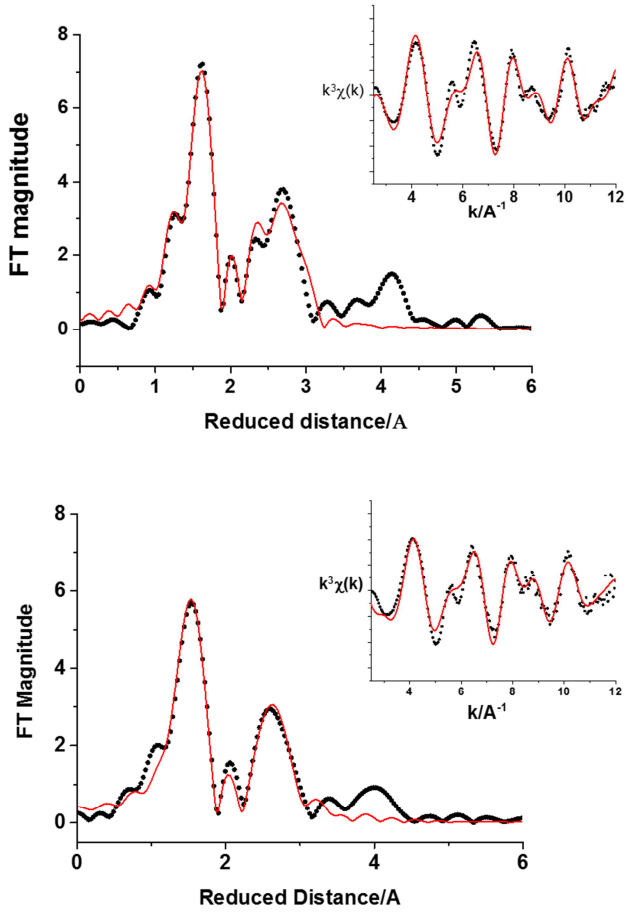

Figure S10. Top: Fourier transform EXAFS spectra of **3** (dotted line) and the best fit (red line); the inset shows the EXAFS data on a wave vector scale weighted by k^3 with respective representation. Bottom: Fourier transform EXAFS spectra of **2** (dotted line) and the best fit (red line); the inset shows the EXAFS data on a wave vector scale weighted by k^3 with respective representation.

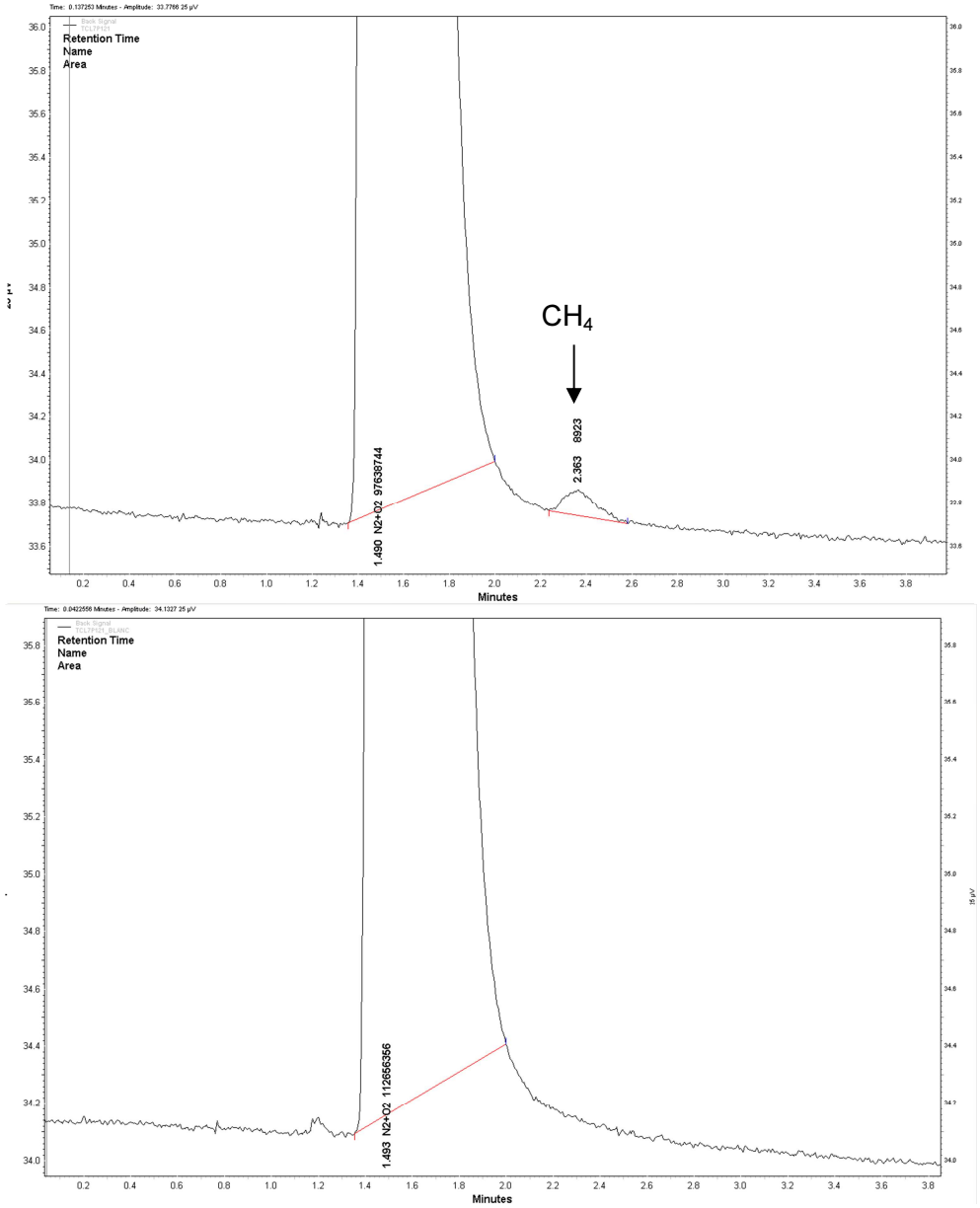

Figure S11. Gas chromatogram (GC-TCD) for the detection of methane released during the reaction of ^{Me}L-N_3 with 1 equi. [$Cu^{I}(CH_3CN)_4$][CF_3SO_3] in acetonitrile at 50 ºC after 7 days (top). For comparison, a blank experiment under analogous conditions without copper is also depicted (bottom).

7. Reaction of 3 with substrates

Analysis of the reaction of 3 with substrates. Once **3** was fully formed, 150 μL of a solution containing the corresponding equivalents of the desired substrate were added in the cuvette. The decay of the band at λ = 710 nm was monitored by UV/vis spectroscopy. After complete decay of this band, the resulting solution was analyzed by NMR and ESI-MS. Trimethoxybenzene (TMB) and triphenylphosphine oxide were used as internal standards in ^{1}H-NMR and ^{31}P-NMR analyses, respectively.

Table S5. Second-order rate constants (k_2, $M^{-1}s^{-1}$) for the reaction of **3** towards substrates together with product analysis and product yields.

Substrate	k_2 ($M^{-1}s^{-1}$)	^{31}P-NMR product (ppm)	ESI-MS m/z product (^{15}N)	Product yield (%)
xanthene	0.009	-	469.31 (471.31)	44
1,4-cyclohexadiene	0.020	-	367.29	-
PPh_3	7.5	26	551.35 (552.34)	41
P^nBu_3	too fast	51	491.35	84
$P(o\text{-}tol)_3$	0.052	17	-	48

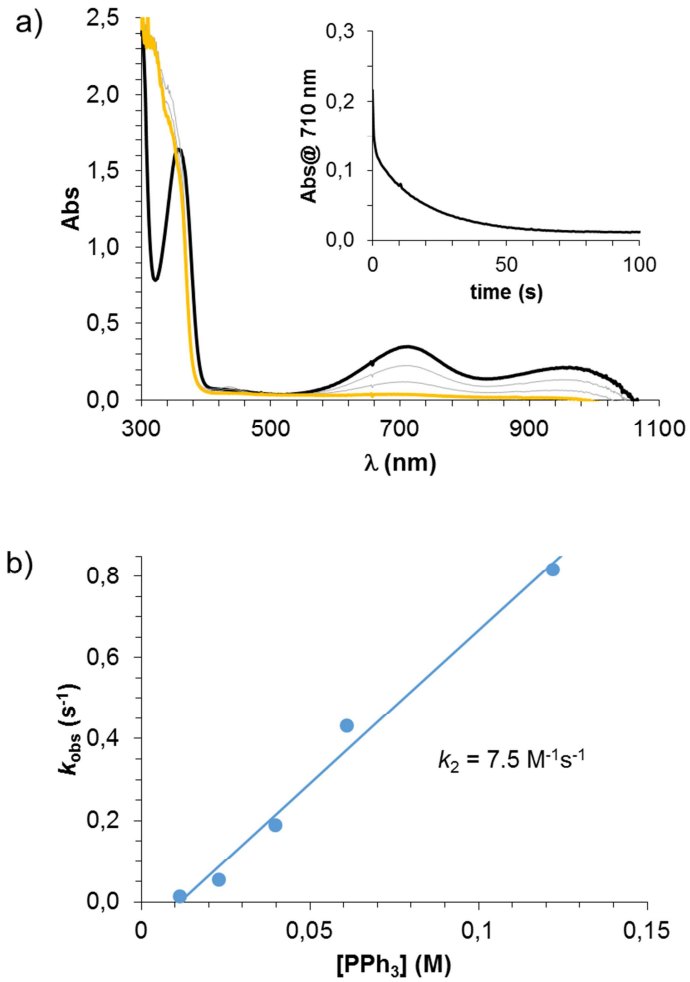

Figure S12. a) UV/vis spectral changes of a solution of **3** upon addition of 15 equiv PPh_3. Experimental reaction conditions: 15 equiv PPh_3 were added at once to a solution of **3** (1.2 mM) in acetonitrile at 25 ºC under Ar and the kinetics were monitored at 710 nm (inset). b) Plot of k_{obs} against substrate concentration for the reaction of **3** (1.2 mM) with triphenylphosphine (PPh_3) in acetonitrile at 25 ºC under Ar.

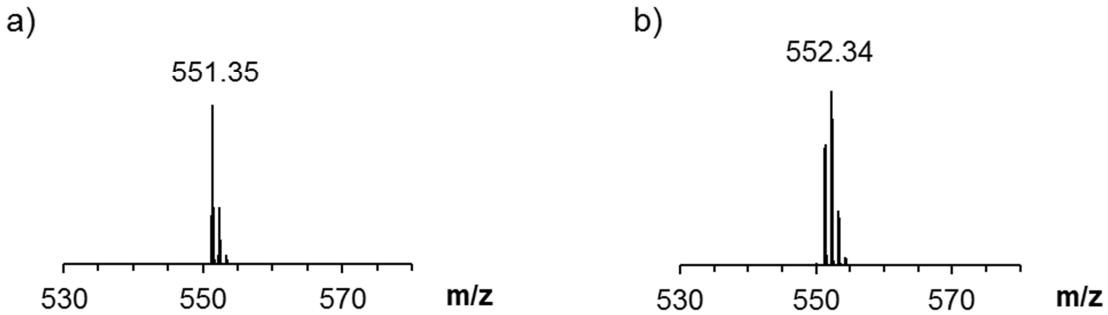

Figure S13. ESI-MS spectrum of the product formed upon reaction of **3** with 5 equiv PPh_3 at 25ºC in acetonitrile (a) and the analogous spectrum starting from 50% ^{15}N-labeled **3** (b).

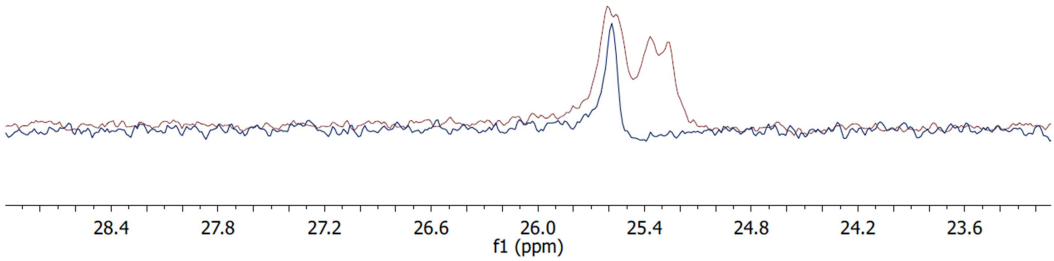

Figure S14. ^{31}P-NMR spectrum of the product formed upon reaction of **3** with 5 equiv PPh_3 at 25ºC in CD_3CN (blue line) and the analogous spectrum starting from 50% ^{15}N-labeled **3** (purple line).

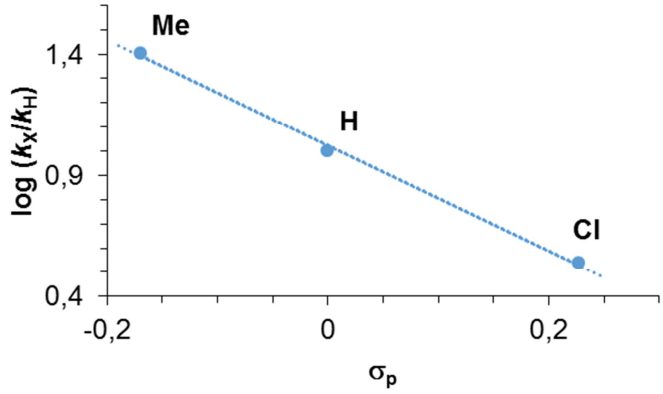

Figure S15. Hammett plot for the reaction of **3** with *para*-substituted triphenylphospines (X = Me, H and Cl) in acetonitrile at 25ºC.

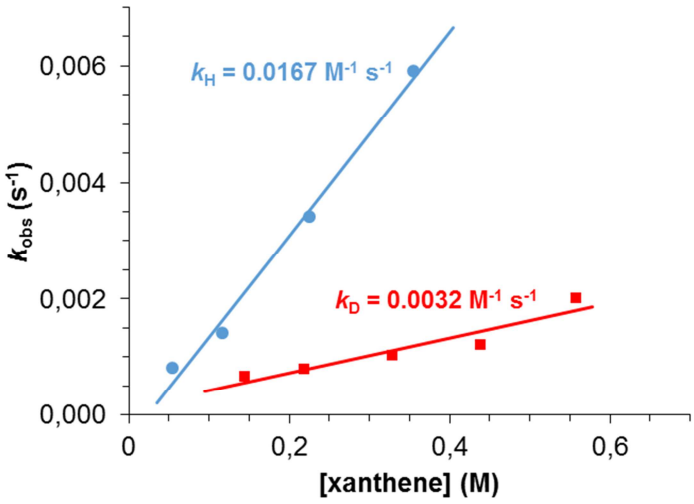

Figure S16. Plot of k_{obs} against substrate concentration for the reaction of **3** with xanthene (blue line) and d_2-xanthene (red line) in acetonitrile at 25 ºC.

8. DFT calculations

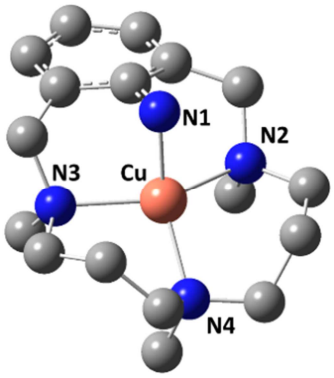

Cu1 N1	1.94	N1 Cu N2	86.3
Cu1 N2	2.16	N1 Cu N3	88.1
Cu1 N3	2.17	N3 Cu N4	100.2
Cu1 N4	2.08	N2 Cu N4	104.2

Figure S17. DFT optimized structure of **3** and selected bond lengths (Å) and angles (º) for this compound.

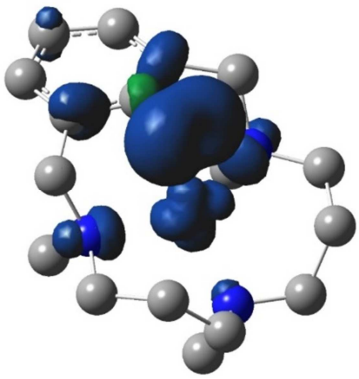

atom	spin density
Cu	0.4
N_{aryl}	1.2
$C_{benzene}$	0.2
N_{CH3}	0.2

Figure S18. Mulliken's spin density of the most relevant atoms for the intermediate **3**, isovalue= 0.005.

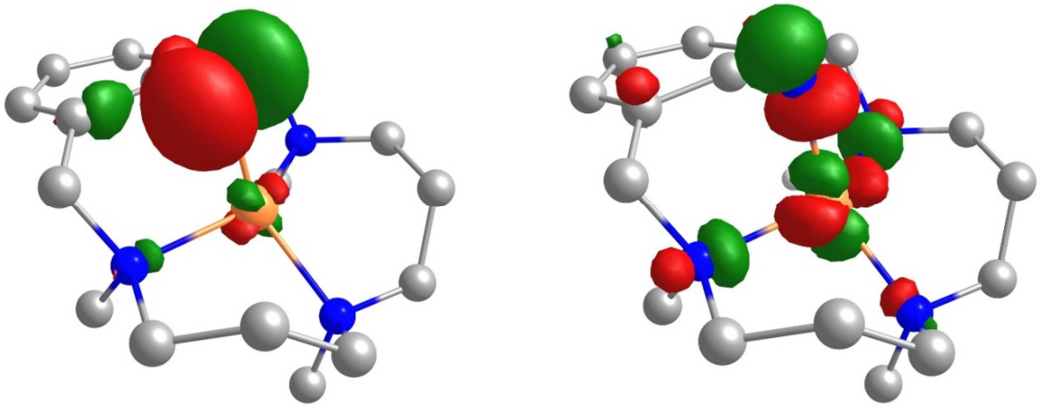

Figure S19. Spin-natural orbitals (SNO) corresponding to **3** (isovalue = 0.062).

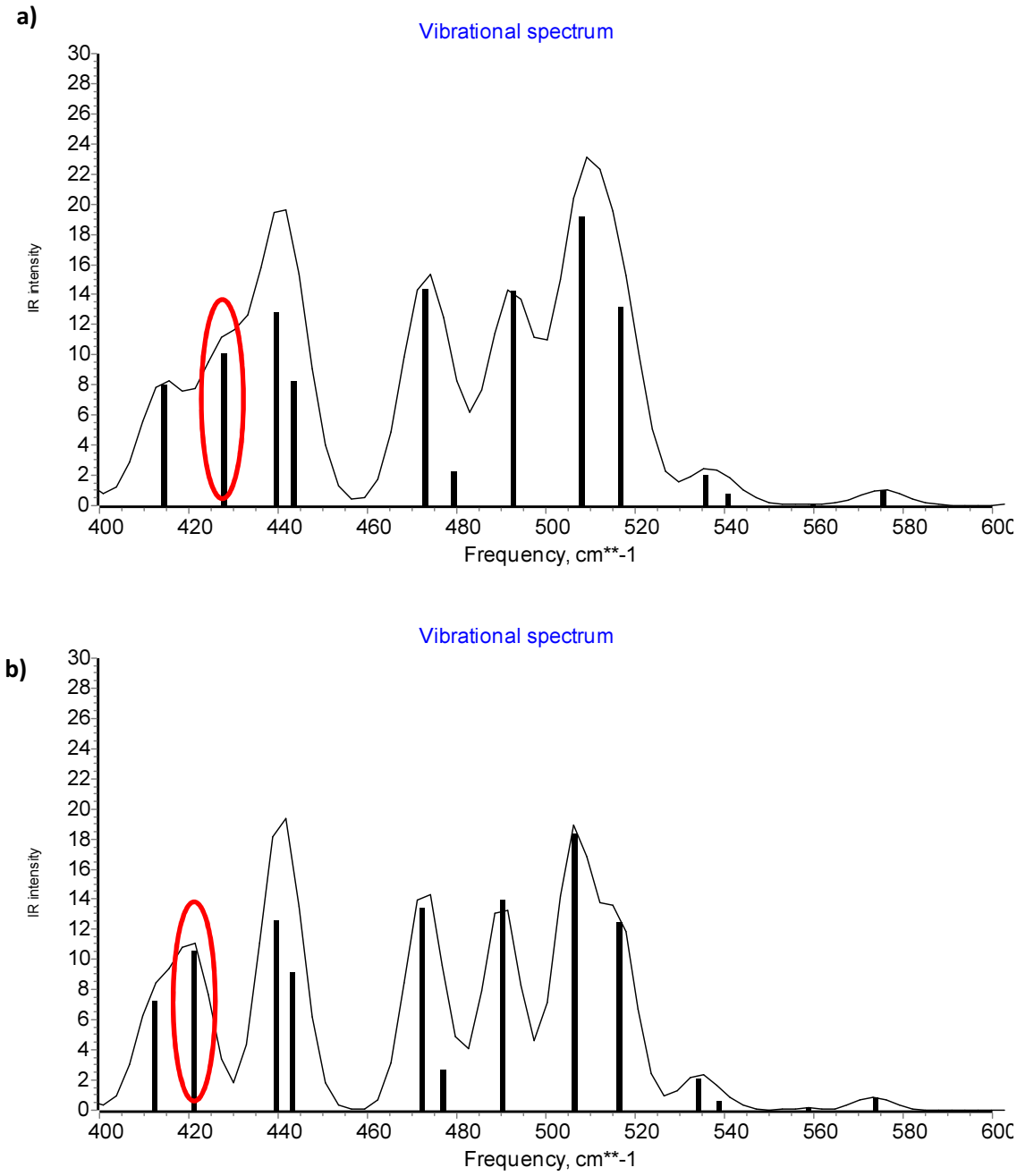

Figure S20. Calculated IR spectrum of compound **3** (a) and its ^{15}N-labeled analogue (b) simulated at 298 K.

Table S6. Cartesian coordinates of intermediate **3**. In parenthesis, the free energies (G) and the zero point energy (E_{ZPE}) (in Hartrees) and the corresponding ground spin state.

$[Cu^{II}(^{Me}L\text{-}N\bullet)]^{+}$ (3) (G= -2523.979296, E_{ZPE} = -2523.931929), triplet

C	-3.57115100	1.18587800	0.23671600	H	3.45221600	0.57623200	-1.35963200
C	-2.38612700	1.19416300	-0.48787100	C	3.01351800	-1.27943700	0.19791300
C	-4.18874800	-0.02245500	0.57982000	C	2.29155700	-2.11806200	-0.86514900
C	-3.54506900	-1.23736400	0.31580900	H	2.97999600	-1.80535800	1.15253700
C	-1.87136500	-0.04750900	-0.94041500	H	4.06948800	-1.16925400	-0.06897300
C	-2.36154800	-1.26857600	-0.41038900	C	1.06240900	-2.92110200	-0.40474200
H	-3.95106400	-2.15979400	0.71771800	H	3.00699700	-2.85407900	-1.24418900
H	-5.11715900	-0.01424500	1.13712900	H	2.02394400	-1.48914300	-1.71992800
H	-3.99382300	2.12327800	0.58292100	H	1.36525900	-3.64377800	0.35778100
N	-0.73660700	-0.05458600	-1.67610600	H	0.69970800	-3.49309000	-1.25909700
C	-1.41713500	2.34346500	-0.62107300	Cu	0.44191400	-0.01881400	-0.13770300
C	-1.40423400	-2.42896500	-0.52917500	H	-1.18534000	-2.63139800	-1.57794400
N	-0.16201500	2.04433400	0.18464300	H	-1.81826900	-3.33671400	-0.08107900
H	-1.85031300	3.28366500	-0.26839400	C	-0.20051600	-2.26285000	1.59750000
H	-1.10471100	2.47274100	-1.65794500	H	-0.43493600	-3.30194200	1.85809100
N	-0.07455200	-2.10285900	0.13247800	H	-0.99608000	-1.61983400	1.97234800
N	2.43851400	0.08935300	0.43003300	H	0.73242200	-1.97974000	2.08164800
C	1.01663800	2.87211000	-0.23821000	C	-0.46737600	2.25043600	1.61661100
C	1.99563000	2.12140900	-1.15187400	H	-0.72540000	3.29790700	1.81407700
H	1.52879000	3.21399600	0.66126000	H	0.39066400	1.97960500	2.22567100
H	0.65719000	3.76508900	-0.75620600	H	-1.31006000	1.62513200	1.90669400
C	2.99149100	1.11369500	-0.53088200	C	2.74270100	0.49341400	1.82106400
H	2.61710800	2.86910900	-1.65433100	H	3.82025100	0.42559400	2.01212100
H	1.42537000	1.62852200	-1.94372000	H	2.21694900	-0.15597100	2.51976300
H	3.79079300	1.65528600	-0.01700500	H	2.43307500	1.52057700	1.9908300

9. References

[1] S. Stoll, A. Schweiger, *J. Magn. Reson.* **2006**, *178*, 42-55.
[2] Demeter, Version 0.9.17, http://bruceravel.github.io/demeter/.
[3] A. L. Spek, *J. Appl. Cryst.* **2003**, *36*, 7-13.
[4] G. M. A. Sheldrick, *Acta Cryst. A* **2008**, *64*, 112-122.
[5] M. J. Frisch, G. W. Trucks, H. B. Schlegel, G. E. Scuseria, M. A. Robb, J. R. Cheeseman, G. Scalmani, V. Barone, B. Mennucci, G. A. Petersson, H. Nakatsuji, M. Caricato, X. Li, H. P. Hratchian, A. F. Izmaylov, J. Bloino, G. Zheng, J. L. Sonnenberg, M. Hada, M. Ehara, K. Toyota, R. Fukuda, J. Hasegawa, M. Ishida, T. Nakajima, Y. Honda, O. Kitao, H. Nakai, T. Vreven, J. A. Montgomery, Jr., J. E. Peralta, F. Ogliaro, M. Bearpark, J. J. Heyd, E. Brothers, K. N. Kudin, V. N. Staroverov, R. Kobayashi, J. Normand, K. Raghavachari, A. Rendell, J. C. Burant, S. S. Iyengar, J. Tomasi, M. Cossi, N. Rega, M. J. Millam, M. Klene, J. E. Knox, J. B. Cross, V. Bakken, C. Adamo, J. Jaramillo, R. Gomperts, R. E. Stratmann, O. Yazyev, A. J. Austin, R. Cammi, C. Pomelli, J. W. Ochterski, R. L. Martin, K. Morokuma, V. G. Zakrzewski, G. A. Voth, P. Salvador, J. J. Dannenberg, S. Dapprich, A. D. Daniels, Ö. Farkas, J. B. Foresman, J. V. Ortiz, J. Cioslowski, D. J. Fox, Gaussian, Inc., Wallingford CT, **2009**.
[6] A. D. Becke, *J. Chem. Phys.* **1993**, *98*, 1372-1377.
[7] A. D. Becke, *J. Chem. Phys.* **1993**, *98*, 5648-5652.
[8] A. Schaefer, C. Huber, R. Ahlrichs, *J. Chem. Phys.* **1994**, *100*, 5829-5835.
[9] A. V. Marenich, C. J. Cramer, D. G. Truhlar, *J. Phys. Chem. B* **2009**, *113*, 6378-6396.
[10] X. Ribas, D. A. Jackson, B. Donnadieu, J. Mahía, T. Parella, R. Xifra, B. Hedman, K. O. Hodgson, A. Llobet, T. D. P. Stack, *Angew. Chem. Int. Ed.* **2002**, *41*, 2991-2994.
[11] A. Casitas, M. Canta, M. Solà, M. Costas, X. Ribas, *J. Am. Chem. Soc.* **2011**, *133*, 19386-19392.